

# Edge-Mediated Annihilation of Vacancy Clusters in Monolayer Molybdenum Diselenide (MoSe<sub>2</sub>) under Electron Beam Irradiation

Xu Zhang, Xiang Zhang, Pulickel M. Ajayan, Jianguo Wen,\* and Horacio D. Espinosa\*

Annihilation of vacancy clusters in monolayer molybdenum diselenide (MoSe<sub>2</sub>) under electron beam irradiation is reported. In situ high-resolution transmission electron microscopy observation reveals that the annihilation is achieved by diffusion of vacancies to the free edge near the vacancy clusters. Monte Carlo simulations confirm that it is energetically favorable for the vacancies to locate at the free edge. By computing the minimum energy path for the annihilation of one vacancy cluster as a case study, it is further shown that electron beam irradiation and pre-stress in the suspended MoSe<sub>2</sub> monolayer are necessary for the vacancies to overcome the energy barriers for diffusion. The findings suggest a new mechanism of vacancy healing in 2D materials and broaden the capability of electron beam for defect engineering of 2D materials, a promising way of tuning their properties for engineering applications.

## 1. Introduction

Structural defects, for example, vacancies, dislocation, and grain boundaries are ubiquitous in materials and play critical roles in controlling material properties.<sup>[1]</sup> This structure-property relationship becomes more dominant when the materials are atomically thin, that is, in 2D materials. For instance, sulfur vacancies in MoS<sub>2</sub> enable n-type doping<sup>[2]</sup> and can modify the electronic,<sup>[2,3]</sup> piezoelectric,<sup>[4]</sup> and optoelectronic<sup>[3,5]</sup> properties

X. Zhang Theoretical and Applied Mechanics Program Northwestern University 2145 Sheridan Rd., Evanston, IL 60208, USA X. Zhang, P. M. Ajayan Department of Materials Science and NanoEngineering Rice University 6100 Main Street, Houston, TX 77005, USA Center for Nanoscale Materials Argonne National Laboratory Lemont, IL 60439, USA E-mail: jwen@anl.gov H. D. Espinosa Department of Mechanical Engineering Northwestern University 2145 Sheridan Rd., Evanston, IL 60208, USA E-mail: espinosa@northwestern.edu

The ORCID identification number(s) for the author(s) of this article can be found under https://doi.org/10.1002/smll.202105194.

DOI: 10.1002/smll.202105194

of the material. Similarly, in hexagonal boron nitride (*h-BN*), the N<sub>B</sub>V<sub>N</sub> (nitrogen vacancy adjacent to a nitrogen located in a boron site) sites enable room-temperature single-photon emission,<sup>[6]</sup> whose spectral distribution can be further modulated by strain.<sup>[7]</sup> Those findings suggest possibilities to tune the properties of 2D materials at will through defect engineering, a promising route to facilitate their applications beyond their intrinsic capabilities.<sup>[2]</sup>

Transition metal dichalcogenides (TMDCs) belong to a group of 2D materials with a formula of MX<sub>2</sub>, where M is a transition metal and X is from the oxygen family. For TMDCs, methods to modulate defects include chemical treatment,<sup>[8]</sup> thermal annealing,<sup>[9]</sup> electron

beam irradiation, [9-15] and plasma irradiation. [16] Specifically, electron beam irradiation with transmission electron microscopy (TEM) allows in situ observation of the creation and subsequent dynamics of defects, thus enabling direct comparison with atomistic simulations for the exploration of the underlying mechanisms. For instance, electron beam irradiation introduces chalcogen (sulfur and selenium) vacancies in monolayer MoS<sub>2</sub>, MoSe2, and WS2 as a result of electron bombardment, and can trigger agglomeration of isolated vacancies into vacancy lines due to reduction in energy. [9,11,15] To date, most studies on defect manipulation with electron beam irradiation report generation and subsequent structural evolution of defects. Electron-beaminduced healing of pre-existing defects, on the other hand, is much less explored. One study by Shen et al. reports healing of nanopores in monolayer MoS<sub>2</sub> as a result of the diffusion of surface adatoms to the vacancy sites.<sup>[14]</sup> With the capability of both creating and healing defects, electron beam irradiation may serve as a versatile technique for defect engineering in TMDCs and other 2D materials. Nevertheless, more experimental and theoretical investigations on electron beam-materials interactions, especially on the healing of defects, are necessary for fulfilling requirements present in engineering applications.

Herein, we report annihilation of vacancy clusters in monolayer MoSe<sub>2</sub> under electron beam irradiation. Through an in situ high-resolution TEM (HRTEM) study, we show that the annihilation of vacancy clusters is achieved by diffusion of vacancies from the clusters to the free edge near the vacancy clusters. Monte Carlo (MC) simulations, enabled by an interatomic potential parameterized for monolayer MoSe<sub>2</sub>, show that it is energetically favorable for the vacancies to locate at the free





edge. We further compute the minimum energy pathway for the annihilation process of a representative vacancy cluster and conclude that electron beam irradiation, as well as pre-stress in the suspended monolayer MoSe<sub>2</sub>, are necessary to trigger the annihilation. Our study reveals a new mechanism of defecthealing in TMDCs and broadens the capability of electron beam for defect engineering of 2D materials.

#### 2. Results and Discussion

#### 2.1. In Situ HRTEM Observation of Vacancy Annihilation

Monolayer MoSe2 flakes were synthesized by chemical vapor deposition (see Experimental Section). The flakes were transferred to Quantifoil holey carbon grids using polystyrene as the transfer polymer.<sup>[17]</sup> HRTEM characterization was conducted at 80 kV acceleration voltage, to reduce beam damage on the monolayer MoSe<sub>2</sub>, inside a FEI Titan 80-300 TEM with an image corrector for reducing both the chromatic and spherical aberrations. The as-synthesized MoSe<sub>2</sub> has a vacancy density that is comparable to CVD-grown MoS2 flakes (see Figure S1, Supporting Information).<sup>[18]</sup> Free edges were created by fracture of flakes during the transfer process (see Figure S2, Supporting Information). No obvious electron beam damage to the monolayer MoSe<sub>2</sub> was observed under an electron dose rate of 1.4 × 10<sup>6</sup> e<sup>-</sup>·nm<sup>-2</sup>·s<sup>-1</sup>. Vacancy clusters start to form under continuous electron irradiation at a dose rate of  $2.9 \times 10^6 \text{ e}^- \cdot \text{nm}^{-2} \cdot \text{s}^{-1}$ (see Figure S3, Supporting Information). We note that the acceleration voltage (80 kV) is below the knock-on threshold voltage to displace Se atoms in MoSe<sub>2</sub> (≈190 kV).<sup>[10]</sup> The creation of vacancy clusters can thus be attributed to 1) ionization damage and 2) electronic excitation in the specimen which is shown to decrease the knock-on threshold voltage for S atoms in MoS<sub>2</sub>.<sup>[12]</sup> Although ionization damage reduces as the acceleration voltage increases, we found more severe beam damage to the monolayer MoSe<sub>2</sub> at 200 kV, suggesting the more dominant electron knock-on damage at such a condition.

Under continuous electron beam irradiation, vacancy clusters start to form in the suspended MoSe<sub>2</sub> monolayer, as shown in Figure 1. The vacancy clusters comprise aggregated Mo and Se2 vacancies and adopt (truncated) triangular shapes similar to those in h-BN.[19] It can be determined from the HRTEM image (Figure 1c,f) that the vacancy clusters possess a zigzag edge (i.e., surface), in agreement with its lower energy in comparison to the armchair edge.<sup>[20]</sup> This conclusion is further corroborated by the FFT pattern (Figure 1a). We compared the FFT pattern to the selected area diffraction pattern of the suspended monolayer MoSe<sub>2</sub> (see Figure S2, Supporting Information) and confirmed that the six spots closer to the central spot correspond to those of the zigzag surface of monolayer MoSe<sub>2</sub>. As shown in Figure 1a, the reciprocal vectors of those spots are perpendicular to the edges of the vacancy clusters, which confirms that those edges have a zigzag termination. Similarly, the free edge adopts a serrated zigzag configuration. Under continuous electron beam irradiation at a dose rate of  $8.17 \times 10^6 \text{ e}^{-1} \cdot \text{nm}^{-2} \cdot \text{s}^{-1}$ , vacancy clusters annihilate or decrease in size (Figure 1b-h, and Movie S1, Supporting Information). Another experiment conducted under the same conditions is

shown in Figure S7, Supporting Information. In the two cases, we observed earlier annihilation of i) vacancy clusters closer to the free edge (vacancy cluster (vc) 3 versus vc2 in Figure 1a, vc7 versus the rest in Figure S7, Supporting Information) and ii) smaller vacancy clusters (i.e., vc3 versus vc4 in Figure 1a) in comparison to other vacancy clusters.

Notably, the annihilation process is accompanied by a decrease of atom columns between the vacancy clusters and the free edge (see Figure S4, Supporting Information). While direct tracing of individual atoms was not conducted due to the inability to capture the fast atomic movements (see Movie S1, Supporting Information), such finding nevertheless implies the diffusion of atoms from the free edge to the vacancy cluster (and diffusion of Mo vacancies and Se2 divacancies in the opposite direction) (see Figure S4, Supporting Information for a detailed explanation). Mechanistically, the annihilation process is distinct from an earlier study on the repair of nanopores in MoS<sub>2</sub> under electron beam irradiation, which is mediated by the diffusion of surface adatoms.<sup>[14]</sup> Our observation suggests that surface annihilation of vacancies, as commonly observed in metallic systems, [21] also exists in 2D materials such as TMDCs. Qualitatively, the annihilation of vacancy clusters can be interpreted as an Ostwald ripening process (i.e., an increase in the size scale of a second phase in the matrix), [22] if one considers the vacancy clusters as the second phase and the free edge as the boundary of a much larger vacancy cluster. Nevertheless, a more quantitative analysis requires consideration of anisotropic edge configurations as well as motion restrictions for each type of atom, as discussed next.

#### 2.2. Monte Carlo Simulations

To explore the driving force for the edge-mediated vacancy annihilation, we simulated such a process with the Monte Carlo (MC) method. The initial structure for the simulation (Figure 2a) was configured to reproduce the experimental observation (see discussion below for different initial edge configurations). Specifically, only Mo monovacancies and Se<sub>2</sub> divacancies (Se atoms above and below the middle Mo layer) were included in the simulations; Se monovacancies and antisite defects, that is, defects in which one atom occupies the site for the other type of atom(s), were not discernable from the HRTEM images and as a result were not introduced. We defined the MC move as swapping between vacancies and their neighboring atoms within a cutoff distance  $d_{\text{max}}$  (60 Å), and adopted the Metropolis MC rules (see Experimental Section, Monte Carlo simulations) for accepting and rejecting the move. The cutoff distance setting accelerates the evolution of the MC simulations and allows us to better mimic the collective motions of atoms as observed experimentally. It allows the MC simulations to sample random moves with higher possibilities of occurrence. However, this algorithm ignores the large reaction barriers imposed by the intermediate configurations (see Section 2.3), and as a result, does not reveal the driving force for the diffusion process. For the evaluation of energy, we used a Tersoff potential that we parameterized for monolayer MoSe2 with an emphasis on nonequilibrium properties, for example, vacancy formation energies, surface energies, and uniaxial tension, etc.[23]

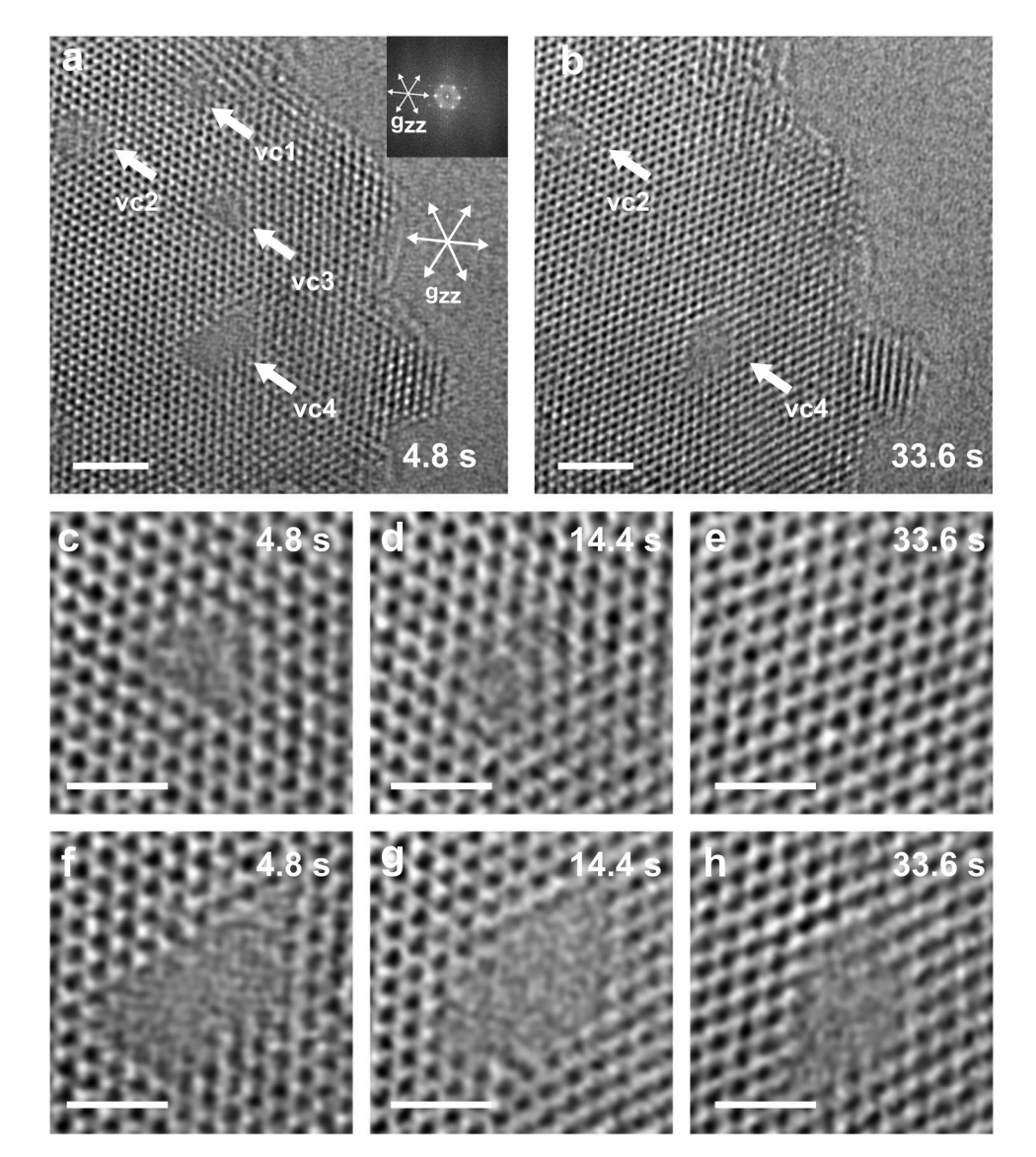
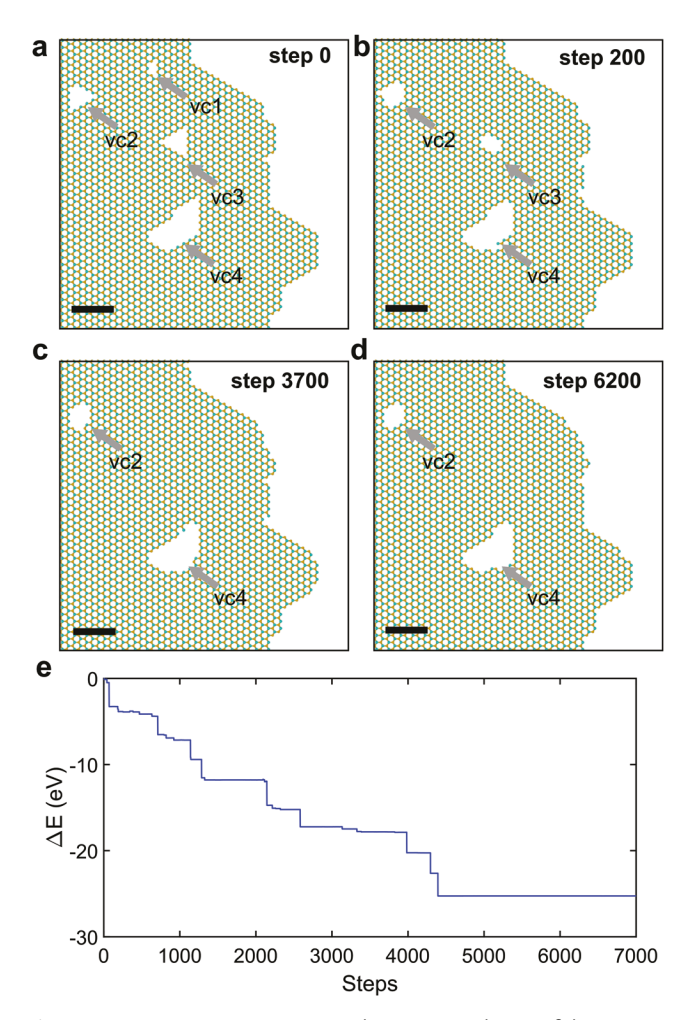


Figure 1. Vacancy annihilation under electron beam irradiation. a,b) Structural evolution of the monolayer  $MoSe_2$  specimen with vacancy clusters (referred as vacancy cluster 1(vc1) to vc4, respectively) near a free edge under continuous electron beam irradiation at a) 4.8 s and b) 33.6 s. vc1 and vc3 annihilate at 33.6 s. The inset image in (a) is the corresponding FFT pattern. The reciprocal vectors corresponding to the zigzag surface were plotted to illustrate that the edges of the vacancy clusters possess zigzag termination. c–e) Structural evolution of vc3 in (a) at c) 4.8 s, d) 14.4 s, and e) 33.6 s. f–h) Structural evolution of vc4 in (a,b) at f) 4.8 s, g) 14.4 s, and h) 33.6 s. The electron dose rate is  $8.17 \times 10^6$  e<sup>-</sup> nm<sup>-2</sup> s. All images were processed with a radial Wiener filter. Scale bars: 2 nm for (a) and (b) and 1 nm for (c–h).

Figure 2 (and Movie S2, Supporting Information) shows a representative MC simulation at 300 K that reproduces the experimental observation: vc1 and vc3 annihilate while the rest two decrease in size, and the free edge contracts. As the annihilation proceeds, the energy of the system decreases in a stepwise manner (Figure 2e). Such data indicates that it is energetically favorable for the vacancies to locate at the free edge in comparison to the vacancy clusters. Moreover, interactions between vacancy clusters were observed (see Movie S2, Supporting Information) in MC simulations. Such interactions are identified in h-BN<sup>[19]</sup> and also in our system between vc1 and vc2 (see Movie S1, Supporting Information).

The aforementioned findings can be explained by the change of coordination number of atoms. In Figure 2, the coordination number of an atom is twice the number of visible bonds since each bond is an overlay of 2 bonds. A Mo (Se<sub>2</sub>) atom(s) has a coordination number of 6 in pristine MoSe<sub>2</sub> and can be either 4 or 2 when they are the terminating atom(s) at the edge. For vacancy sites in a cluster, the coordination numbers can be 4, 2, and 0, corresponding to 60° corners, other sites at the cluster edge, and inside the cluster, respectively (see Figure S5, Supporting Information). An increase in coordination number decreases the energy and is therefore favorable. The annihilation process always initiates from the 60° corners of the vacancy cluster, advances to other sites at its edge, and



**Figure 2.** A representative Monte Carlo (MC) simulation of the vacancy annihilation process at 300 K. a–d) Simulation snapshots at a) step 0, b) step 200, c) step 3700, and d) step 6200, respectively. The initial structure (a) is constructed from Figure 1a by mapping the atom columns. Extra atoms are put in the simulation system (not shown in the figures) at the top, left, and bottom of the region of interest to exclude boundary effects. Mo atoms are colored cyan, and Se atoms are colored orange. Scale bar: 2 nm. e) Change of the total energy as a function of MC steps.

terminates when no swap attempt can increase or maintain the coordination number. Larger vacancy clusters have more sites with low coordination numbers (<4) and as a result are less likely to completely annihilate. Vacancy clusters away from the free edge have more restricted access to atoms at the free edge and therefore are less likely to annihilate.<sup>[24]</sup> We note that temperature within commonly reachable range (<1500 K) has a minimum effect on the annihilation due to the large increase in energy when coordination number decreases (see Section 2.3).

The free edge in Figure 2 possesses either a Mo- or Se-zigzag configuration with a coordination number of 4. Besides those two types, the Mo-Klein edge (see Figure S6, Supporting Information) is also found to be stable in nanoporous MoS<sub>2</sub> films grown with molecular beam epitaxy under high Mo flux.<sup>[25]</sup> It can be created by removing the outermost Se atoms in Sezigzag edge, leaving exposed Mo atoms with a coordination number of 2. As shown in **Table 1**, converting 50%<sup>[26]</sup> of the

**Table 1.** Probability of annihilation for the vacancy clusters under different initial edge configurations. The zigzag-only structure (Figure 2a) contains Mo- and Se-zigzag edges, while the zigzag and Mo-Klein configuration (Figure S6, Supporting Information) contains a third type: the Mo-Klein edge. Specifically, the ratio between Se-zigzag and Mo-Klein is set to be 1:1. The probability was calculated from 60 simulations with different random seeds.

Vacancy clusters	Zigzag only	Zigzag and Mo-Klein
vcl	1	1
vc2	0	0.07
vc3	0.03	0.97
vc4	0	0

Se-zigzag edge to the Mo-Klein edge increases the probability of annihilation for vc2 and vc3, highlighting its notable effect on the annihilation.

We note a low acceptance rate of the MC simulations for diffusion events with an increase of energy, that is,  $\Delta E > 0$ . To verify that this is not due to the parametrization of the interatomic potential, we compared results of several simplified vacancy diffusion events, predicted by the interatomic potential, against first-principle simulations. As shown in Figure S9 and S10, Supporting Information, first-principle simulations for vacancy diffusion instances with  $\Delta E > 0$  also predict  $\Delta E$  values that are much higher than thermal energy  $(k_bT)$ , which agrees with results obtained from the parameterized interatomic potential. Hence, the low acceptance rate is embedded in the as-studied system and further justifies our selection of the cutoff distance, which accelerates the process.

### 2.3. Minimum Energy Path for a Proposed Annihilation Process

The MC simulations are limited in revealing the kinetics of the annihilation process, for example, diffusion barriers for the vacancy. Such information is embedded in the kinetic Monte Carlo method, [27] which is not applied herein due to the complexities of our system in both composition and configuration. Indeed, the MC simulations resemble the experimental observations better and circumvent several technical challenges one would encounter using kMC simulations, as detailed in SI, Supporting Note 1. To complement MC simulations, we explored the annihilation kinetics of a specific vacancy cluster, that is, vc1 (Figure 3), as means to extrapolate a general picture for our system. The complete annihilation process of vc 1 is hypothesized to be achieved by the sequential annihilation of each individual vacancy site (i.e., two Mo vacancies and one Se2 vacancy), initiating at either Mo vacancy at the corner of vc1. For each individual vacancy site, its annihilation is hypothesized to be composed of a sequence of vacancy-hopping events. For instance, the Mo vacancy (Figure 3a), in each hopping event, diffuses to its nearest neighboring site until it reaches the edge and collectively moves the entire layer of Mo atoms inward (see Movie S3, Supporting Information for a movie of this process). We computed the minimum energy path (MEP) of each vacancyhopping event with the climbing image nudged elastic band (CI-NEB) method<sup>[28]</sup> and combined them into one curve

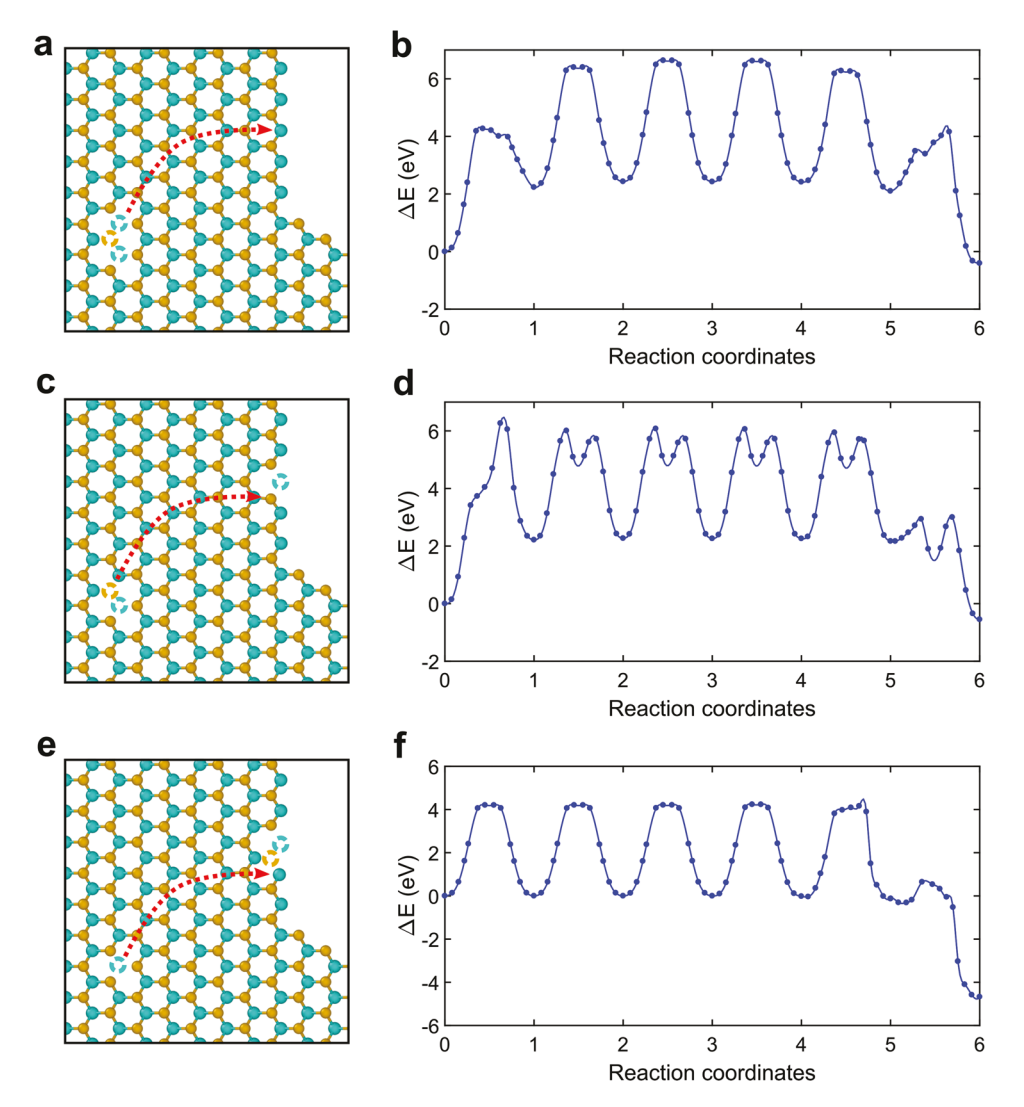


Figure 3. Proposed vacancy annihilation process for vc1. a) Atomic snapshot and b) minimum energy pathway (MEP) of a Mo vacancy undergoing sequential hopping from the vacancy cluster to the free edge, which causes the vacancy site to annihilate. The snapshot (a) corresponds to reaction coordinates (RC) = 0 in (b). c) Atomic snapshot and d) minimum energy pathway of the sequential hopping of the  $Se_2$  vacancy. The snapshot (c) corresponds to RC = 6 in (b) and RC = 0 in (d). e) Atomic snapshot and f) minimum energy pathway of the sequential hopping of the Mo vacancy. The snapshot (e) corresponds to RC = 6 in (d) and RC = 0 in (f). Complete annihilation of vc1 (RC = 6 in (f)) decreases the energy of the system by 5.7 eV. In (a), (c), and (e), the arrow indicates the hopping direction and destination of the vacancy, and the dashed circles represent vacancies. Mo atoms and vacancies are colored cyan, and Se atoms and vacancies are colored orange. For better visualization of the diffusion path of the individual vacancies, other vacancy clusters were not shown in (a), (c), and (e).

(Figure 3b). The system for the CI-NEB simulation is identical to the MC simulations. We note that the local stress field may be affected by the free edge, as has been shown to contribute to vacancy dynamics in suspended monolayer MoS<sub>2</sub>.<sup>[11]</sup> Similarly, vacancy clusters may interact through their stress fields, as inferred from studies in graphene, which show that vacancies and divacancies stress fields are equivalent to an edge dislocation dipole.<sup>[29]</sup> To this end, energy minimization is conducted during each step of the CI-NEB simulation to account for the above elastic driving forces. The MEP varies according to local atomic configurations, and the completion of this process results in a slight decrease of energy due to local structural relaxation. Following the annihilation of the Mo vacancy, the Se<sub>2</sub> divacancy (Figure 3c) and the Mo vacancy

(Figure 3e) annihilate in a similar manner, as shown by their MEP, Figure 3d and f, respectively. The biggest decrease in energy is observed in Figure 3f when the net coordination number of the system increases by 4. This agrees with the MC simulations and confirms that the annihilation is energetically favorable.

The activation barriers of vacancy-hopping are 0.77, 3.70, and 6.29 eV for a Se<sub>2</sub> divacancy, and 0.24, 1.89, 3.59, and 4.00 eV for a Mo vacancy, all of which are larger than thermal energy at room temperature ( $\approx$ 0.026 eV). This suggests the necessity of other energy sources in assisting the barrier-hopping events. Electron beam irradiation is one such source, as has been found to introduce vacancy migration in several 2D materials including graphene, [30] h-BN, [19] MoS<sub>2</sub>, [10,11,31] and MoSe<sub>2</sub>, [9] The





maximum energy that can be transferred to an atom from an electron in an elastic scattering is given as:<sup>[32]</sup>

$$E_{\text{max}} = \frac{2ME_0 \left( E_0 + 2m_0 c^2 \right)}{2ME_0 + \left( M + m_0 \right)^2 c^2} \tag{1}$$

where M is the mass of the atom,  $E_0$  is the incident beam energy,  $m_0$  is the mass of an electron, and c is the speed of light. At 80 keV electron beam energy,  $E_{\text{max}}$  for Mo and Se atom is 1.97 and 2.40 eV, which suggests that elastic scattering due to electron beam irradiation is not sufficient for the vacancies to overcome the energy barriers in all the scenarios of Figure 3. We identify pre-stress in the suspended membrane as another source of energy for barrier-hopping events of the vacancies. To quantify the magnitude of strain in the as-observed system, we adopted the structural template matching method, developed by Madsen et al., [33] which uses the equilibrium lattice constant as the reference and is capable of revealing absolute strains. An average compressive strain of 9.3% and 10.3% (see Figure S8b,c, Supporting Information) was identified along the armchair and zigzag direction, respectively. The compressive strain should facilitate the diffusion of vacancies to the free edge of the specimen, analogously to the Nabarro-Herring creep mechanism in metals.<sup>[34]</sup> It has also been shown that the pre-stress in suspended monolayer MoS2 can lead to spontaneous crack propagation when the monolayer is punctured by the electron beam.[35]

For the as-studied atomic systems, we note size limitations of first-principle NEB simulations in capturing the effect of the free edge and other vacancy clusters on vacancy-hopping. To verify the accuracy of NEB simulations based on the interatomic potential, we constructed simplified atomic models to compare results obtained from the interatomic potential against those from first-principle NEB simulations. The simplified models include the following cases for a Mo monovacancy and  $\mathrm{Se}_2$  divacancies: diffusion (of the vacancy) to the free edge, diffusion from the vacancy cluster, and diffusion within pristine MoSe<sub>2</sub>. As shown in Figure S9 and S10, Supporting Information, deviations of energy barriers from the first-principle results, in the range of 0.12-2.49 eV, were identified for the parameterized interatomic potential. Given that the as-adopted interatomic potential is more accurate than existing ones for monolayer MoSe<sub>2</sub> on large-deformation pathways,<sup>[23]</sup> we attribute such discrepancies to intrinsic limitations on the transferability of interatomic potentials. However, such deviations do not affect the conclusion that other sources of energy, besides the electron beam irradiation, are necessary for vacancy-hopping since the energy barriers computed from first-principle simulations are still higher than the energy provided by the electron beam as computed from Equation (1).

#### 3. Conclusions

We report HRTEM observation of edge-mediated annihilation of vacancy clusters in monolayer MoSe<sub>2</sub> under electron beam irradiation at room temperature. We conduct MC simulations and confirm that it is energetically favorable for the vacancies

to locate at the free edge in comparison to the vacancy clusters as the former configuration provides a larger coordination number. The kinetics of the annihilation is explored on a proposed annihilation pathway for a vacancy cluster. The large activation barrier in comparison to thermal energy suggests the necessity of electron beam irradiation and pre-stress in the suspended monolayer in triggering the annihilation process.

It has been shown that the electronic properties of TMDCs can be tuned by modifying the edge configuration and vacancy concentrations. The Mo-zigzag and Mo-Klein edges in MoS<sub>2</sub> are metallic in comparison to the semiconducting MoS<sub>2</sub> basal plane,<sup>[25]</sup> and sulfur vacancies in MoS<sub>2</sub> can introduce n-type doping.<sup>[2,3]</sup> To this end, our findings reveal a new interaction mechanism between the electron beam and TMDCs, which may be used to fine-tune the properties of TMDCs and other 2D materials through defect-engineering. Moreover, in the context of fracture of 2D materials, our findings suggest possible interactions between vacancies and cracks that may alter crack propagation and fracture properties of 2D materials. In the absence of electron beam irradiation, such interactions may resemble the creep mechanism in metallic materials and may affect the fracture toughness of 2D materials.

We show that the vacancy annihilation process preferably initiates from atomic sites with lower coordination numbers. The atomic configurations with lower coordination numbers, for example, vacancies, can be introduced by post-treatment such as electron beam irradiation and also during the growth of the material. For instance, Zhou et al. report edge reconstructions in CVD-grown monolayer MoS2 flakes under a Morich growth environment.[36] The reconstructed edges contain monosulfur vacancies and unsaturated Mo atoms. Those surface configurations may further facilitate the annihilation process, similar to the Mo-Klein edge herein studied. We did not observe such an edge reconstruction herein probably due to different growth environments. We leave such investigation to future studies. We restrict the computational studies herein to Se<sub>2</sub> divacancies because they are readily visible in the HRTEM images (see Figure 1 and Figure S7, Supporting Information), which allows us to compare our simulation results directly to those images. While Se monovacancies appear to be more abundant in CVD-grown MoSe2 samples, they are not easily discernable in the aforementioned HRTEM images because the difference in brightness, which is used to discern Se monovacancies under TEM (see Figure S1, Supporting Information), is not trustworthy when the entire atomic structures undergo major structural evolution. Such a task (and the study of Se monovacancy diffusion) is more suitable to be conducted under STEM with the utilization of Z-contrast.<sup>[37]</sup> Given the numerous configurations and diffusion pathways for Se monovacancies in the system studied herein, direct experimental observation of Se monovacancy diffusion pathway, possibly with STEM, is necessary to reveal single vacancy diffusion mechanism. We leave such investigation to future studies.

#### 4. Experimental Section

Sample Preparation: MoSe<sub>2</sub> was synthesized by chemical vapor deposition. MoO<sub>3</sub> and Se powders were used as the precursors, and placed at the center and upstream of a tube furnace, respectively. SiO<sub>2</sub>/

Si was used as the substrate and placed on the top of  $MoO_3$  powder. The growth was conducted at 750 °C for 15 min with  $H_2/Ar$  (15% $H_2$ ) as the carrier gas.

The as-synthesized  $MoSe_2$  was transferred from the growth substrate to Quantifoil holey carbon grids using polystyrene (PS) as the transfer polymer. [17] 1.8 g of Polystyrene ( $M_w = 280\,000$  g mol<sup>-1</sup>) was dissolved in 20 mL toluene at  $\approx 50$  °C. The solution was spin-coated onto the growth substrate (3500 rpm, 60 s) followed by a 15 min baking process at 80 °C. Next, a water droplet was added onto the substrate and the PS film was poked from the edge to let water penetrate through the substrate/film interface and release the PS film. The PS film with  $MoSe_2$  flakes was picked up and attached onto the quantifoil holey carbon grids, followed by a baking process at 80 °C for 1 h and then at 150 °C for 30 min. PS was removed by rinsing with toluene. Only a mild rinsing was conducted as it was found that excessive rinsing disintegrated the holey carbon film. As such, polymer residues were found on some transferred flakes.

In Situ HRTEM Characterization: HRTEM characterization was conducted with the chromatic aberration-corrected TEM (FEI Titan 80–300 ST with an aberration corrector for both the spherical and chromatic correction) at an acceleration voltage of 80 kV. Prior to imaging, the specimen was heated in a vacuum pump station with a vacuum pressure below  $1\times10^{-7}$  torr at  $\approx\!130~^{\circ}\text{C}$  for 2 h to reduce hydrocarbon. The images were taken with spherical and chromatic aberration corrected such that  $C_{\text{s}}<5~\mu\text{m}$ , and  $C_{\text{c}}<5~\mu\text{m}$ . The images were processed with a radial Wiener with an information limit of  $0.4\times$  maximum frequency.

Monte Carlo Simulations: The Monte Carlo (MC) simulations were carried out in a canonical system (constant number of atoms, volume, and temperature). The initial simulation system was configured to match the experimental observation. Since the exact edge configuration (for both the vacancy cluster and the free edge) was not discernable from the HRTEM images, variations in edge configurations were introduced according to those identified in monolayer MoS<sub>2</sub>.<sup>[25]</sup> A padding layer of pristine MoSe<sub>2</sub> was included at the top, bottom, and left of the system in Figure 2a to eliminate the boundary effects. In each MC step, each vacancy was attempted to swap with a corresponding atom(s), that is, a Mo atom for Mo vacancy and Se2 (above and below the Mo layer) for Se<sub>2</sub> divacancy, within a cutoff distance  $d_{max}$ . After the swap, the energy of the new system was evaluated by running a single point calculation using a Tersoff potential parameterized for the mechanical and thermal properties of monolayer MoSe<sub>2</sub>.<sup>[23]</sup> The probability for accepting or rejecting the swap attempt follows the Metropolis MC,[38] namely,

$$p = \exp\left(-\frac{\Delta E}{k_b T}\right) \qquad \text{(for } \Delta E > 0\text{)}$$

$$p=1$$
 (for  $\Delta E \le 0$ ) (3)

In Equations (2) and (3),  $\Delta E$  is the change of the total energy (ignoring thermal vibration) after the swap attempt,  $k_b$  is the Boltzmann constant, and T is the temperature. For cases where  $\Delta E > 0$ , a random number  $\xi \in [0.0, 1.0)$  was generated and the attempt was accepted if  $\xi < p$ . With the above setting, the swap move satisfies the requirement of ergodicity and detailed balance. Throughout the simulation, the energy of the system, the success rate, and the configuration of the system were recorded periodically for the subsequent analysis. The Large-Scale Atomic/Molecular Massively Parallel Simulator (LAMMPS) software package<sup>[39]</sup> was used for energy calculations.

Mininum Energy Path Calculation: The minimum energy pathway was computed by climbing image NEB method in LAMMPS.<sup>[28]</sup> The system configuration was identical to that of the MC simulations. Fourteen replicas including the initial and final configurations were created for each individual hopping event in Figure 3a. The energy and force cutoff for the minimization was selected as 0.01 eV and 0.01 eV Å<sup>-1</sup>, respectively. The spring constant for the nudging force was set as 0.1 eV Å<sup>-1</sup>. The

energy of the system was computed with the parameterized Tersoff potential. First-principle simulations were conducted with SIESTA<sup>[40]</sup> and the setup was documented in our earlier work.<sup>[23]</sup>

# **Supporting Information**

Supporting Information is available from the Wiley Online Library or from the author.

# **Acknowledgements**

The authors acknowledge the support of the National Science Foundation, through award CMMI 1953806, and computational resources provided by the Center of Nanoscale Materials at Argonne National Laboratory, as well as the Quest High Performance Computing Cluster at Northwestern University. This work was performed, in part, at the Center for Nanoscale Materials, a U.S. Department of Energy Office of Science User Facility, and supported by the U.S. Department of Energy, Office of Science, under Contract No. DE-AC02-06CH11357. X.Z. acknowledges the helpful discussion from Songting Cai on interpreting the HRTEM results, and Hoang Nguyen on conducting the first-principle minimum energy path calculations.

#### **Conflict of Interest**

The authors declare no conflict of interest.

#### **Author Contributions**

H.D.E. formulated the investigation and guided the research. Xu Zhang transferred the synthesized  $\mathsf{MoSe}_2$  flakes onto the TEM grid, analyzed the HRTEM images, and conducted Monte Carlo simulations and the minimum energy path calculations. J.W. formulated the investigation, carried out the HRTEM characterization, and offered suggestions on interpreting the HRTEM images. Xiang Zhang synthesized the  $\mathsf{MoSe}_2$  flakes. P.M.A. guided the synthesis. All authors contributed to the writing of the manuscript and discussion of results.

# **Data Availability Statement**

The data that support the findings of this study are available from the corresponding author upon reasonable request.

#### **Keywords**

2D materials, electron irradiation, high-resolution transmission electron microscopy, Monte Carlo simulations, vacancies

Received: August 27, 2021 Revised: October 20, 2021 Published online:

<sup>[1]</sup> D. Hull, D. J. Bacon, Introduction to Dislocations, Vol. 37, Elsevier,

<sup>[2]</sup> J. Jiang, T. Xu, J. Lu, L. Sun, Z. Ni, Research 2019, 2019, 4641739.

<sup>[3]</sup> H. Nan, Z. Wang, W. Wang, Z. Liang, Y. Lu, Q. Chen, D. He, P. Tan, F. Miao, X. Wang, ACS Nano 2014, 8, 5738.





- [4] S. A. Han, T. H. Kim, S. K. Kim, K. H. Lee, H. J. Park, J. H. Lee, S. W. Kim, Adv. Mater. 2018, 30, 1800342.
- [5] P. Lin, L. Zhu, D. Li, Z. L. Wang, J. Mater. Chem. C 2019, 7, 14731.
- [6] T. T. Tran, K. Bray, M. J. Ford, M. Toth, I. Aharonovich, Nat. Nanotechnol. 2016, 11, 37.
- [7] G. Grosso, H. Moon, B. Lienhard, S. Ali, D. K. Efetov, M. M. Furchi, P. Jarillo-Herrero, M. J. Ford, I. Aharonovich, D. Englund, *Nat. Commun.* 2017, 8, 705.
- [8] Y. Meng, C. Ling, R. Xin, P. Wang, Y. Song, H. Bu, S. Gao, X. Wang, F. Song, J. Wang, npj Quantum Mater. 2017, 2, 16.
- [9] J. Lin, S. T. Pantelides, W. Zhou, ACS Nano 2015, 9, 5189.
- [10] H.-P. Komsa, J. Kotakoski, S. Kurasch, O. Lehtinen, U. Kaiser, A. V. Krasheninnikov, Phys. Rev. Lett. 2012, 109, 035503.
- [11] H.-P. Komsa, S. Kurasch, O. Lehtinen, U. Kaiser A. V. Krasheninnikov, *Phys. Rev. B* 2013, 88, 035301.
- [12] S. Kretschmer, T. Lehnert, U. Kaiser, A. V. Krasheninnikov, *Nano Lett.* 2020, 20, 2865.
- [13] Y.-C. Lin, D. O. Dumcenco, Y.-S. Huang, K. Suenaga, Nat. Nanotechnol. 2014, 9, 391.
- [14] Y. Shen, T. Xu, X. Tan, L. He, K. Yin, N. Wan, L. Sun, Adv. Mater. 2018, 30, 1705954.
- [15] J. Zhao, H. Nam, T. H. Ly, S. J. Yun, S. Kim, S. Cho, H. Yang, Y. H. Lee, Small 2017, 13, 1601930.
- [16] J. P. Thiruraman, P. Masih Das, M. Drndić, Adv. Funct. Mater. 2019, 29, 1904668
- [17] A. Gurarslan, Y. Yu, L. Su, Y. Yu, F. Suarez, S. Yao, Y. Zhu, M. Ozturk, Y. Zhang, L. Cao, ACS Nano 2014, 8, 11522.
- [18] J. Hong, Z. Hu, M. Probert, K. Li, D. Lv, X. Yang, L. Gu, N. Mao, Q. Feng, L. Xie, J. Zhang, D. Wu, Z. Zhang, C. Jin, W. Ji, X. Zhang, J. Yuan, Z. Zhang, *Nat. Commun.* 2015, 6, 6293.
- [19] N. Alem, R. Erni, C. Kisielowski, M. D. Rossell, P. Hartel, B. Jiang, W. Gannett, A. Zettl, *Phys. Status Solidi RRL* 2011, 5, 295.
- [20] Y. Yang, X. Li, M. Wen, E. Hacopian, W. Chen, Y. Gong, J. Zhang, B. Li, W. Zhou, P. M. Ajayan, Adv. Mater. 2017, 29, 1604201.
- [21] R. Balluffi, Metall. Trans. B 1982, 13, 527.
- [22] I. M. Lifshitz, V. V. Slyozov, J. Phys. Chem. Solids 1961, 19, 35.
- [23] X. Zhang, H. Nguyen, J. T. Paci, S. K. Sankaranarayanan, J. L. Mendoza-Cortes, H. D. Espinosa, npj Comput. Mater. 2021, 7, 1.

- [24] This is controlled by an arbitrary cutoff distance dmax but nevertheless reflects the real physics.
- [25] X. Zhao, D. Fu, Z. Ding, Y.-Y. Zhang, D. Wan, S. J. Tan, Z. Chen, K. Leng, J. Dan, W. Fu, *Nano Lett.* 2018, 18, 482.
- [26] We note that the ratio is 70% in MoS2 films grown with high Mo flux. (see Zhao et al., Nano Lett. 2018, 18, 482.). Since such a Mo-rich condition was not applied in our synthesis protocol, we decreased that ratio to 50%
- [27] a) C. C. Battaile, Comput. Methods Appl. Mech. Eng. 2008, 197, 3386;
   b) Y. Cai, S. Chen, J. Gao, G. Zhang, Y.-W. Zhang, Nanoscale 2019, 11, 20987.
- [28] a) G. Henkelman, H. Jónsson, J. Chem. Phys. 2000, 113, 9978;
  b) G. Henkelman, B. P. Uberuaga, H. Jónsson, J. Chem. Phys. 2000, 113, 9901.
- [29] A. Carpio, L. Bonilla, Phys. Rev. B 2008, 78, 085406.
- [30] J. Kotakoski, C. Mangler, J. C. Meyer, Nat. Commun. 2014, 5, 3991
- [31] J. Hong, Y. Pan, Z. Hu, D. Lv, C. Jin, W. Ji, J. Yuan, Z. Zhang, Nano Lett. 2017, 17, 3383.
- [32] Y. Wang, T. Wakasugi, S. Isobe, N. Hashimoto, S. Ohnuki, Microscopy 2014, 63, 437.
- [33] J. Madsen, P. Liu, J. B. Wagner, T. W. Hansen, J. Schiøtz, Adv. Struct. Chem. Imaging 2017, 3, 16.
- [34] T. H. Courtney, Mechanical Behavior of Materials, Waveland Press, Long Grove, IL 2005.
- [35] S. Wang, Z. Qin, G. S. Jung, F. J. Martin-Martinez, K. Zhang, M. J. Buehler, J. H. Warner, ACS Nano 2016, 10, 9831.
- [36] W. Zhou, X. Zou, S. Najmaei, Z. Liu, Y. Shi, J. Kong, J. Lou, P. M. Ajayan, B. I. Yakobson, J.-C. Idrobo, *Nano Lett.* 2013, 13, 2615.
- [37] M. Mahjouri-Samani, L. Liang, A. Oyedele, Y.-S. Kim, M. Tian, N. Cross, K. Wang, M.-W. Lin, A. Boulesbaa, C. M. Rouleau, *Nano Lett.* 2016, 16, 5213.
- [38] D. Frenkel, B. Smit, Understanding Molecular Simulation: From Algorithms to Applications, Vol. 1, Elsevier, Amsterdam 2001.
- [39] S. Plimpton, J. Comput. Phys. 1995, 117, 1.
- [40] J. M. Soler, E. Artacho, J. D. Gale, A. García, J. Junquera, P. Ordejón, D. Sánchez-Portal, J. Phys.: Condens. Matter 2002, 14, 2745.